# Design of a Wireless Power and Data Transfer System for pH Sensing inside a Small Tube

Fatemeh Mohseni<sup>1α</sup>, Paul Marsh<sup>1α</sup>, Filippo Capolino<sup>1</sup>, J.-C. Chiao<sup>3</sup>, Hung Cao<sup>1,2\*</sup>

<sup>1</sup>Electrical Engineering and Computer Science Department, University of California Irvine, USA

<sup>2</sup>Biomedical Engineering Department, University of California Irvine, USA

<sup>3</sup>Electrical and Computer Engineering Department, Southern Methodist University, USA

fatemem@uci.edu, marshp@uci.edu, f.capolino@uci.edu, jchiao@smu.edu, \*hungcao@uci.edu, \*ORCID:

0000-0003-4197-7208

α- equal contributions

Abstract— This work presents a passive wireless measurement system for potentiometric chemical probes inside a small laboratory tube. An inductively coupled link is utilized with DC-to-frequency signal transduction via load modulation. The wireless power transfer part of the system features advantageous flexibility in coil separation distances and stability in the frequency providing maximum power transfer, as evidenced by the couple-mode theory analysis. We then demonstrate continuous pH sensing through a cap for a 50-ml centrifuge tube. Instrumentation and resultant data are presented, showcasing excellent linearity and tunable outputs. Our approach and system architecture can be used for numerous passive wireless potentiometric sensing applications in both laboratory and industry settings, as well as other wireless sensing systems, with minor circuit modification.

Keywords—wireless power transfer, inductive coupling, antenna theory, chemical and biological sensing, pH sensor.

## I. INTRODUCTION

Wireless power transfer (WPT) has paved the way for advances in portable electronic devices applied to a host of applications, from wirelessly powered laptops [1] to biomedical devices for organ or wound monitoring [2]. Wireless power transfer methods can be categorized into two main classes: radiative and non-radiative. Radiative WPT, like far-field or RF broadcast techniques, is based on propagating electromagnetic waves carrying energy. Although this is suitable for transferring data, there are some disadvantages for transferring power. In far-field techniques, the efficiency is highly dependent on the directivity of the transmitter. Even in RF broadcasting methods, where this is solved by omnidirectional propagation, the transferred power drops rapidly with a  $1/r^2$  distance dependency. Non-radiative methods, like inductive coupling based on resonance, are getting more and more popular for near-field applications as it has been demonstrated that two resonant objects exchange energy more efficiently [3]. Design and optimization of wireless power transfer systems featuring inductive links have been studied extensively [4, 5] and are used broadly.

In sensing applications, WPT allows for long-term, continuous measurement [2]. Solution pH is one popular and crucial measurement for chemical and biological processes and *in-situ* environmental monitoring. Conventional pH meters, using dual-junction AgCl glass electrodes, have been widely

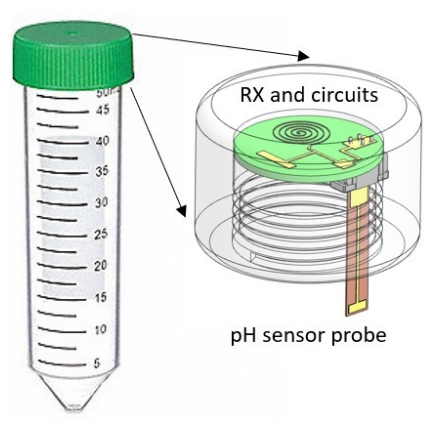


**Fig. 1.** Passive wireless pH sensing inside a small tube. The system method can be expanded for multi-modal sensing inside one tube, as well as for simultaneous real-time measurements in multiple tubes.

used due to their high precision and reliability but are bulky, expensive, and application-limited as compared to contact thin film probes. These shortcomings have limited their uses in emerging micro-systems embedded with biosensors and bioelectronics [6]. Another issue for pH and other ionic measurements is that opening containers exposes samples to air, thereby altering sample constituents and reaction outcomes. Sampling within enclosed containers alleviates these concerns. To this end, a passive wireless pH sensing system, inside a small laboratory tube, using inductive coupling WPT and backscattering communication, has already been demonstrated in [7], as well as the thin-film pH sensor probes.

In this work, we carried out in-depth investigations of a wireless power and data transfer system for the potentiometric measurement of pH. Circuits for power amplification, signal transduction and load modulation are presented in detail. The conceptual design of this system can be seen in **Fig. 1**.

## II. SYSTEM AND DESIGN

The concept for power transfer and data communication is shown in **Fig. 2**. In this system, the output power of a switching power amplifier is transferred via magnetically coupled coils. After harvesting the power and regulating to desired DC levels, it is fed to a pH sensor connected to the signal transduction unit.

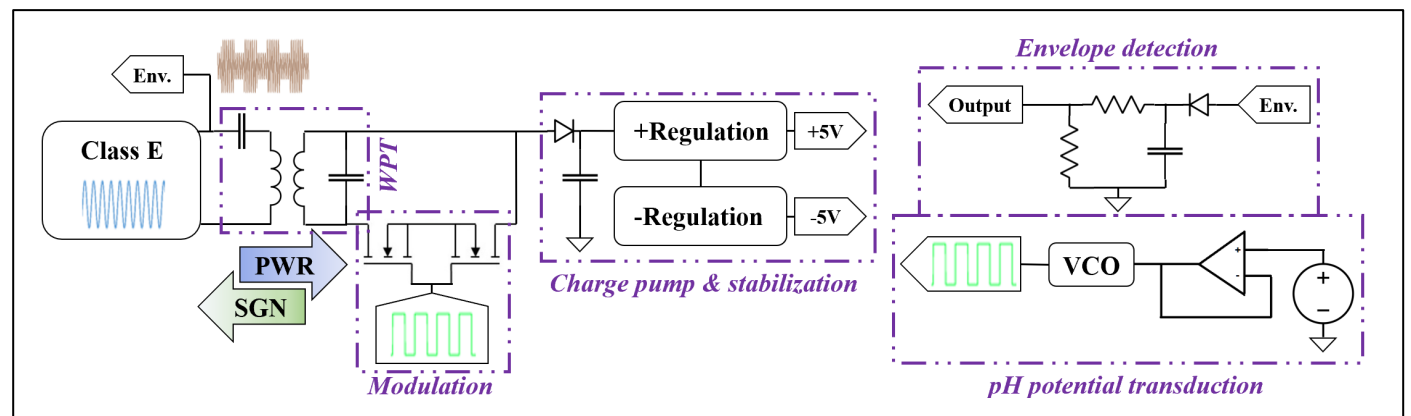


**Fig. 2**. Schematic diagram for the wireless power transfer and load-modulation signal transduction. Logical segregation of the subsystems is highlighted with dashed boxes.

The measured data are load-modulated in frequency onto the carrier signal, which would be then demodulated at the transmitter side for data acquisition.

## A. Class-E amplifier

The high efficiency Class-E amplifier delivers a 1-W output power at 1 MHz of carrier frequency [8] (Fig. 2). The out-of-phase voltage and current ensure a high efficiency. Higher harmonics are filtered, as the magnetic coupling and capacitance act as a filter. The amplifier requires phase tuning to maintain this out-of-phase requirement. The tuning considerations also include the load impedance seen from the amplifier side, as the magnetic coupling behaves equivalently to a transformer, and the spacing between coils varies the mutual inductance. A low-impedance load would cause an excessive current in the amplifier and create significant thermal losses. This load sensitivity is valuable for load modulation schemes, where the impedance change at the receiver modulates the transferred signal generated by the amplifier.

## B. Inductive link

The transmitter (TX) and receiver (RX) coils, contained in the block labeled "WPT" in Fig. 2, are magnetically coupled to transfer power. The coupling coefficient depends on the coil geometry and spacing, and coil tuning is performed with a variable capacitor. This tuning and pairing can be analyzed with coupled-mode theory (CMT), where the differential equations are generally intended to determine the energy exchange between two resonating objects. The CMT formalism simplifies the differential equations compared to that of traditional circuit theories, as it only considers one first order equation for each resonant object [9]. CMT describes the resonators' signal amplitudes as:

$$\dot{a}_m(t) = (j\omega_m - \gamma_m)a_m(t) + \sum_{n \neq m} jK_{mn}a_n(t) + F_m(t)$$
(1)

where  $a_m$  (m = 1,2) is the complex mode amplitude in each resonator (subscripts 1 and 2 refer to the TX and RX resonators, respectively); therefore,  $|a_m|^2$  refers to the energy stored in the  $m^{\text{th}}$  resonator. A time evolution of  $a_m \propto e^{j\omega t}$  is implicitly assumed for steady-state analysis. The resonator frequency of

the uncoupled  $m^{th}$  resonator is  $\omega_{0m}$ . The factor  $K_{mn}=\omega_{0m}k_{mn}/2$ , with  $k_{mn}=M_{mn}/\sqrt{L_mL_n}$ , is the coupling coefficient between resonators. Finally,  $\gamma_m=G_m\omega_{0m}\sqrt{L_m/C_m}$  is the loss factor for each resonator.

Power transfer efficiency for a system of two coils with the same resonant frequency is calculated as

$$\eta_t = \frac{\gamma_2 |a_2|^2}{\gamma_1 |a_1|^2 + \gamma_2 |a_2|^2} = \frac{\gamma_2}{\gamma_1} \frac{K_{12}^2}{K_{12}^2 + \gamma_1 \gamma_2}$$
(2)

Therefore, coupling factor changes due to changes in TX-RX coil gap alter the amplitude and efficiency of the transferred power. Off resonance, the system operating frequency is not equal to the resonant frequency of each coil and power transfer efficiency is decreased. Therefore, maximum power transfer occurs in the resonant state. In practice, the operating frequency should be restricted to roughly the resonant frequency.

In the WPT substage, the TX side inductance was  $8.6~\mu H$ , as realized with a 16-turn solenoid coil with a radius of 18~mm and a series C of 2.2~nF. The RX side inductance was  $8.2~\mu H$ , with a shunt C of 2.7~nF. In practice, the complete system resonates at 980~kHz.

# C. Energy harvesting

The "charge pump and stabilization" substage highlighted in Fig. 2 contains the energy harvesting circuitry. To drive the load, the power transferred from TX to RX must be rectified. A half-wave diode rectifier, with capacitive smoothing, was used to provide inputs to a positive voltage regulator. A TLV76701 linear regulator, with Zener diode input protection, was used. The use of a linear regulator was a compromise between power efficiency, low dropout voltage, and low noise. Since significant power could be transferred over the inductive link, the efficiency penalty for using a linear regulator was deemed acceptable. The TLV76701 provides a +5 V output.

To provide for symmetric voltage rails, a MAX1681ESA switching voltage converter was used to provide a -5 V rail on the board. It switches at a frequency well above the signal frequency range (approximately 500 kHz), so any induced noise would not affect the signal. The actual modulation frequency range is discussed in Section E.

## D. Potentiometric pH sensing and voltage follower stage

Sensing of pH is performed by measurement of potential changes at a metal oxide surface. The circuitry shown here is intended to measure potential difference between an iridium oxide (IrOx) working electrode (WE) and a reference electrode (RE), such as silver chloride [10] or other material. Use of these probes requires an investigation of their output potential range.

The standard Nernst equation at room temperature suggests a sensitivity of 59.1 mV/pH if a single electron is transferred during the redox reaction of interest (in this case, hydrogen ion transfer):

$$E = E^{0} - \frac{RT}{nF} \ln(Q) = E^{0} - \frac{0.0591 \, V}{n} \times pH \tag{3}$$

In this equation, n denotes the number of electrons transferred. Since IrOx surface redox states in hydrous films can vary, however, n can be less than one [11]. Therefore, hydrous films tend to have slightly higher sensitivity, closer to 75 mV/pH or more [10].

This information allows us to calculate the window of operation (therefore, power supply voltages necessary) for the potentiometric substage and its included voltage follow opamps: sensitivity multiplied by pH range determines the voltage span, and empirically determined formal potentials ( $E^0$ ) determine the offset. As an example, calculation, a 75-mV/pH probe in contact with an electrolyte ranging from pH 2 to pH 10 results in a voltage swing of 600 mV, empirically found to be centered anywhere from -0.4 to +0.4 V; this necessitates a  $\pm 1$ V DC measurement window.

Rather than supply the voltage follower op-amps with  $\pm 1V$  power, however, they are supplied with  $\pm 5V$  power. This is because  $\pm 5V$  is already generated for driving the modulation transistors, so the system is simplified by not adding secondary power regulators. Therefore, the voltage follower op-amps are supplied with higher supply voltages than are required for electrode output.

#### E. Signal transduction

pH measurement data correspond to a calibrated relationship between pH level and DC voltage. However, DC amplitude modulation of the carrier is subject to drift and power rail considerations, so a frequency modulation scheme was chosen to avoid these issues. To transfer pH-to-voltage readings, a voltage-controlled oscillator (VCO) was used to convert voltage levels to oscillation frequencies, thereby changing the calibration relationship to pH-to-frequency. The LTC6990 VCO was used, fed by a 3-stage voltage follower and amplifier chain ("pH potential transduction" in Fig. 2). The oscillation frequencies can be tuned, allowing widening range to increase modulation resolution while avoiding the carrier frequency.

Following VCO oscillation, the signal is then transferred from RX to TX coil via inductively coupled load. Two NMOSFET devices, tied source-to-source and placed in series with the rectifier output, directly alter the RX circuit load impedance when driven by VCO oscillation. The source-to-source configuration was chosen to ensure that the FET body

diodes cannot be forced into reverse breakdown by LC tank voltages; this ensures drain current passes only when the gates are being driven past  $V_{th}$ . NMOSFET BSZ900's were chosen for their low on-resistance (<100 m $\Omega$ ) and gate threshold voltage ( $V_{th} = 4$  V,  $I_D = 20$  A @  $V_{GS} = 5$  V).

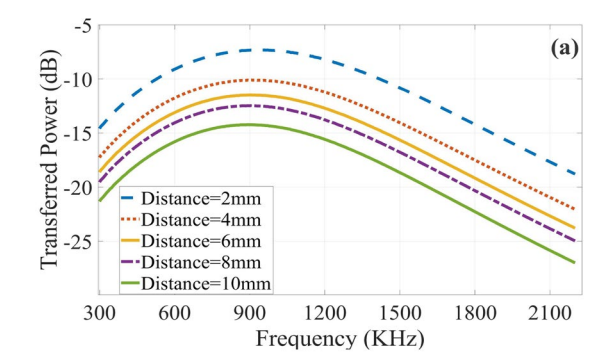
## F. Data acquisition

On the RX side, an 8 - 24 kHz information signal generated by VCO modulates the 980 kHz carrier signal on the TX side. The signal features a modulation index of roughly 0.1, resulting in a single-side modulation amplitude of approximately 0.5 V. Then, this signal is demodulated with an AM demodulator consisting of a diode and RC filter ("envelope detection" substage of **Fig. 2**). The modulation frequency information is measured by time-windowed counting.

#### III. RESULTS AND DISCUSSION

Fig. 3(a) demonstrates transferred power between two coils measured by a vector network analyzer with multiple coil spacings. Fig. 3(b) shows the mutual coupling  $k_{mn} = M_{mn}/\sqrt{L_m L_n}$  values calculated for each distance.

The mutual coupling  $k = M/\sqrt{L_{RX}L_{TX}}$  values were calculated for each distance. As can be seen, the frequency at which the transferred power peaks does not change significantly with changes in coil-to-coil distance. This is owing to the direct-fed structure that maintains stability over various distances. With direct-fed coils, load and source resistances decrease the quality factor, hence making the



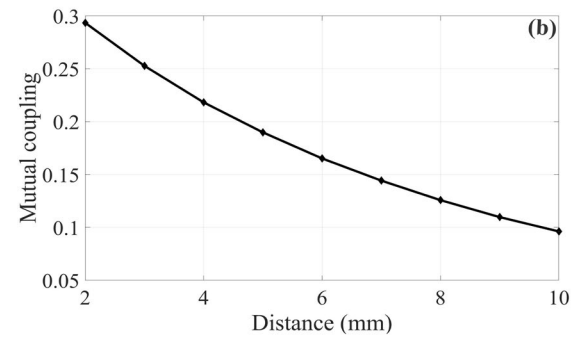


**Fig. 3.** (a) Coupling investigation results demonstrating measured transmission coefficient in power ratio at different coil-to-coil separation distances. (b) Mutual coupling factor  $k_{12}$  change over the coil-to-coil distance.

system resonant frequency less sensitive to distance change

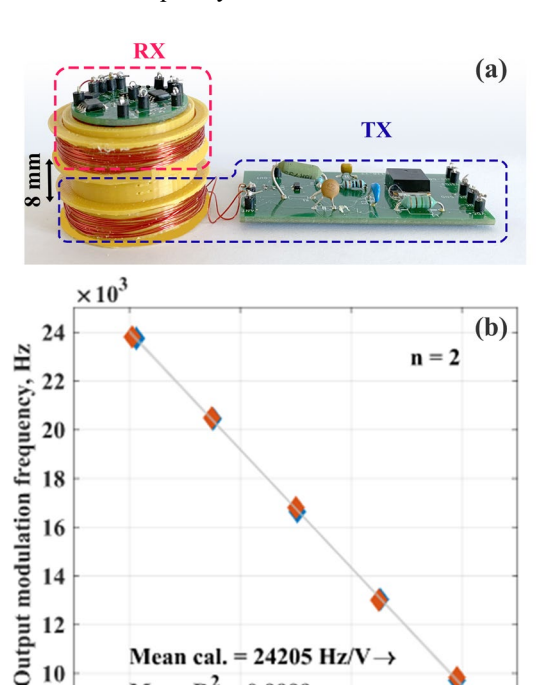


Fig. 4. System overview and test results. (a) TX and RX assemblies. TX includes the Class-E amplifier and envelope detector. RX consists of energy harvester, pH potential transduction circuitry, and load modulation circuitry. (b) Results of two IrOx probe tests. These tests were performed with respectively independent calibrations. Buffer input voltage is the potential produced directly by the pH sensor. Output modulation is the counted frequency value after demodulation at the envelope detector.

Buffer input, Volts

Mean cal. = 24205 Hz/V→

0.4

0.6

Mean  $R^2 = 0.9999$ 

0.2

12

10

8

0

[12]. Due to this relative carrier-frequency insensitivity with distance variations, the system can easily be operated as a handheld reader for embedded measurement devices.

Shown in Fig. 4(a) is a fully fabricated system, including a spool for coil winding and controlled separation. The transmitter and receiver coils feature a coupling factor  $k \approx 0.25$ . The receiver board was designed with a circular shape for use in a sealed, laboratory sample tube [7]. Direct calibration via demodulated signals is demonstrated in Fig. 4(b) for two different sensor probes. The modulator was tuned to provide output frequencies in the range of 8 to 24 kHz when supplied with pH sensor potentials from 0 to 0.6 V. As expected, the output is linear with regards to the potential.

#### IV. CONCLUSIONS

In this work, we present detailed implementation of a passive wireless pH sensing system for continuous monitoring of dynamic processes inside a small laboratory tube. We focused on important components and features of both the inductive coupling-based wireless link and electronic circuitry energy harvesting, amplifying, modulating, demodulating. Specifically, the employed frequency-shift modulation ensures the signal-to-noise ratios are not affected by wireless power transfer distances. RX-received power is regulated for use across the device, ensuring precise measurement. Therefore, our simple, yet efficient, electronics design can be used in many other applications which interrogate highly precise DC sources. Future work will delve more deeply into the simplification of the RX circuitry and into improving the power efficiency and frequency of operation with respect to distance variations, as well as the operation with multiple RXs. Our system architecture can be adapted and expanded for multi-modal sensing in one tube as well as simultaneous monitoring of multiple tubes in real time. The TX can be also connected to a cloud server so that pH and/or other quantities such as temperature, glucose, lactate, just to name a few, can be monitored anytime, anywhere without opening the tube.

#### ACKNOWLEDGMENT

The authors wish to acknowledge financial support under the NSF CAREER #1917105 and the startup fund from the Henry Samueli School of Engineering, UC Irvine.

#### REFERENCES

- A. P. Sample, D. A. Meyer, and J. R. Smith, "Analysis, Experimental Results, and Range Adaptation of Magnetically Coupled Resonators for Wireless Power Transfer," IEEE Transactions on Industrial Electronics, vol. 58, pp. 544-554, 2011.
- H. Cao, V. Landge, U. Tata, Y. S. Seo, S. Rao, S. J. Tang, et al., "An implantable, batteryless, and wireless capsule with integrated impedance and pH sensors for gastroesophageal reflux monitoring," IEEE Trans Biomed Eng, vol. 59, pp. 3131-9, Nov 2012.
- X. Wei, Z. Wang, and H. Dai, "A Critical Review of Wireless Power Transfer via Strongly Coupled Magnetic Resonances," Energies, vol. 7, pp. 4316-4341, 2014.
- A. Hajiaghajani and S. Ahn, "Single-Sided Near-Field Wireless Power Transfer by A Three-Dimensional Coil Array," Micromachines (Basel), vol. 10, Mar 21 2019.
- M. Kiani, Ieee, M. Ghovanloo, and Ieee, "The Circuit Theory Behind Coupled-Mode Magnetic Resonance-Based Wireless Power Transmission," IEEE Trans Circuits Syst I Regul Pap, vol. 59, pp. 2065-2074, Sep 2012.
- H. E. Amor, A. B. Kouki, P. Marsh, K. T. Kim, and H. Cao, "Development of a novel miniaturized LTCC-based wireless pH sensing system," in SENSORS, 2016 IEEE, 2016, pp. 1-3.
- P. Marsh, Y. Zhuang, Z. Xu, L. Heine, and H. Cao, "Sample Tube pH Monitoring via Passive Powering and Communication," in 2019 IEEE SENSORS, 2019, pp. 1-4.
- [8] S. Aldhaher, P. C.-K. Luk, and J. F. Whidborne, "Tuning Class E Inverters Applied in Inductive Links Using Saturable Reactors," IEEE Transactions on Power Electronics, vol. 29, pp. 2969-2978, 2014.
- S. Assawaworrarit, X. Yu, and S. Fan, "Robust wireless power transfer using a nonlinear parity-time-symmetric circuit," Nature, vol. 546, pp. 387-390, Jun 14 2017.
- [10] P. Marsh, L. Manjakkal, X. Yang, M. Huerta, T. Le, L. Thiel, et al., "Flexible Iridium Oxide Based pH Sensor Integrated With Inductively Coupled Wireless Transmission System for Wearable Applications," IEEE Sensors Journal, vol. 20, pp. 5130-5138, 2020.
- [11] P. Steegstra and E. Ahlberg, "Influence of oxidation state on the pH dependence of hydrous iridium oxide films," Electrochimica Acta, vol. 76, pp. 26-33, 2012.
- [12] J. Kim, J. Kim, S. Kong, H. Kim, I.-S. Suh, N. P. Suh, et al., "Coil Design and Shielding Methods for a Magnetic Resonant Wireless Power Transfer System," Proceedings of the IEEE, vol. 101, pp. 1332-1342, 2013.